Structure and charge transfer dynamics of the $(Ar–N_2)^+$ molecular cluster

R. Candori, S. Cavalli, F. Pirani, and A. Volpi
INFM and Dipartimento di Chimica, Università di Perugia, 06123 Perugia, Italy

D. Cappelletti
INFM and Dipartimento di Ingegneria Civile ed Ambientale, Università di Perugia, 06125 Perugia, Italy

P. Tosi and D. Bassi
INFM and Dipartimento di Fisica, Università di Trento, Trento, Italy

(Received 16 July 2001; accepted 6 September 2001)

In this paper we have investigated the interaction potential and the charge transfer processes at low collision energies in the $(Ar–N_2)^+$ system. The angular dependence of the lowest doublet potential energy surfaces (PES), correlating with $Ar^+(^2P_j)–N_2$ and $Ar–N_2^+(^2\Sigma,^2\Pi)$, has been given in terms of spherical harmonics, while the dependence on the intermolecular distance has been represented by proper radial coefficients. Such coefficients, which account for van der Waals, induction, charge transfer, and electrostatic contributions, have been predicted by empirical correlation formulas. The PES so obtained have been employed to calculate cross sections for the charge transfer process $Ar^+ + N_2 \rightarrow Ar + N_2^+$ at low collision energy ($E \leqslant 2$ eV). A good agreement between calculated and experimental cross sections is obtained by assuming that the duration of the nonadiabatic transition has to match the time required for the molecular rearrangement into the final vibrational state. As a consequence the efficient formation of product ions into specific vibrational states is limited to well defined ranges of impact parameters. This treatment leads to a unified description of the major experimental findings. © *2001 American Institute of Physics.* [DOI: 10.1063/1.1413980]

I. INTRODUCTION

The reaction,

$$Ar^+(^2P_j) + N_2(X,^1\Sigma_g^+)(\nu=0) \rightarrow Ar + N_2^+(X,^2\Sigma_g^+)(\nu'), \quad (1)$$

and its reverse have been widely studied becoming a paradigm of the charge transfer processes. Since these are the simplest chemical reactions, occurring without atomic rearrangement, they have been thoroughly investigated both experimentally and theoretically. Unfortunately a complete understanding of the underlying microscopic mechanisms is still lacking. This study represents an effort to provide a detailed representation of the interaction and a unified description of major experimental findings on these processes.

The energy dependence of the integral cross section for charge transfer reaction (1) was measured in a crossed beam experiment.[1] Despite the fact that the reaction is exothermic by 0.179 eV, the observed behavior is typical of an endothermic process. With increasing collision energy, the cross section rises from an apparent threshold of about 0.1 eV and declines at energies larger than about 1 eV. The explanation of such behavior relates to the state selectivity of the process. The most abundant product at low collision energy is $N_2^+(X\,^2\Sigma_g^+)$ in the first vibrational level $\nu'=1$,[2,3] which is endothermic by 0.092 eV. At higher collision energy, all energetically accessible vibrational states of $N_2^+(X\,^2\Sigma_g^+)$ are populated and each of them is scattered into a specific angular cone.[4] This characteristic behavior is observed only in a relatively narrow energy range centered around 1 eV.[5,6] Outside this energy range, forward-scattered $N_2^+(X\,^2\Sigma_g^+)(\nu'=1)$ is the only detectable reaction product. These observations have puzzled researchers for the last twenty years and stimulated many experimental investigations by different laboratories which result today in a large body of detailed information. State-to-state cross sections[7–11] and the rotational energy distribution of the products[12] have been measured. Additional information concerns reaction rates at very low temperatures,[13,14] the photodissociation dynamics of the reaction intermediate complex $(Ar–N_2)^+$ (Ref. 15) and the influence of rotational[16] and spin–orbit[17–19] energy on the reactivity.

On the theoretical side, several studies[20–28] have tried to elucidate specific aspects of this charge transfer process, although a consistent and complete treatment of the dynamics is still missing. In particular, details of the interaction, which closely affect the collisional dynamics at low energy, are unknown and neither the energy dependence of the integral cross section[1] nor the angular dependence of the differential cross section[4] has yet been explained.

In this paper we present a new evaluation of the interaction potential energy surfaces, PES, for the $(Ar–N_2)^+$ system based on a proper blend of angular momenta coupling schemes[29] and empirical correlation formulas.[30–34] Dynamical calculations using the obtained PES reproduce well the experimental energy dependence of the integral cross section for the charge transfer reaction $Ar^+ + N_2 \rightarrow Ar + N_2^+$ for collision energies from thermal up to 2 eV. The model shows that, for a given product vibrational state, the yield varies strongly with the impact parameter and is thus correlated to the scattering angle. Efficient production is limited to a well-defined range of impact parameter in which the duration of the nona-

diabatic transition matches the time required for molecular rearrangement into the final vibrational state.

In the next section the method adopted to determine the interaction potential in the $(Ar–N_2)^+$ complex is described. In the same section the relative role of interaction components of different nature is also discussed. The low lying potential energy surfaces so obtained are reported in Sec. III, where the role of the vibronic states is also discussed. The collisional dynamics is treated in Sec. IV and the representation of the nonadiabatic coupling at crossings between vibronic surfaces is given in Sec. V. Comparison with the experiments and conclusions follow in Secs. VI and VII. Finally an appendix describes the parameterization of the various interaction components.

II. THE INTERACTION IN THE CHARGE TRANSFER COMPLEX

In the $(Ar–N_2)^+$ system, electron exchange between the two near resonant charge states, $Ar^+ + N_2$ and $Ar + N_2^+$, plays a fundamental role in the stabilization of the complex. For this reason an accurate description of the interaction requires a proper representation of the states involved as well as of their couplings. In particular, it is important to account for the spin–orbit interaction, the molecular anisotropy and the electronic anisotropy related to the open-shell nature of Ar^+. For this purpose, the potential is expanded in a series of bipolar spherical harmonics, representing the angular dependence, and radial coefficients describing the intermolecular distance dependence of the atom–molecule interaction. Such coefficients involve the specific contributions of different components of the interaction, namely, dispersion, induction, electrostatic, and repulsion. Such a method has been recently exploited in the description of prototype open shell atom–molecule systems, such as $F–H_2$ and $Cl–H_2$,[29] and will here be applied to the present case. It should be noted that charge exchange plays a more important role in the present system than in those studied by Ref. 29; indeed, in the present case it has been assumed to be the most important coupling term between the states involved, whereas in $F–H_2$ and $Cl–H_2$ it was included as a perturbative effect. The radial coefficients have been obtained by empirical correlation formulas,[30–34] and their knowledge allows us to evaluate directly the specific role of each component in the collision dynamics.

A. Representation of the interaction

In this section the methodology used to compute the potential energy surfaces, permitting the dynamical treatment of the $Ar^+ + N_2$ charge transfer reaction (see Sec. III), is described. A diabatic representation of the electronic Hamiltonian matrix H is constructed and then diagonalized for each nuclear configuration to obtain the adiabatic potentials. The geometry of the $(ArN_2)^+$ complex is conveniently described in terms of the Jacobi coordinates R, r, and θ, where R is the distance of the atom from the center of mass of the molecule, r is the bond distance of the diatom, and θ is the angle included between the vectors **R** and **r** (see Fig. 1).

The approach of $Ar^+(^2P_j)$ to the $N_2(X\,^1\Sigma_g^+)$ molecule gives rise to three electronic states which correlate asymptotically, in order of increasing energy, to the following reactant channels:

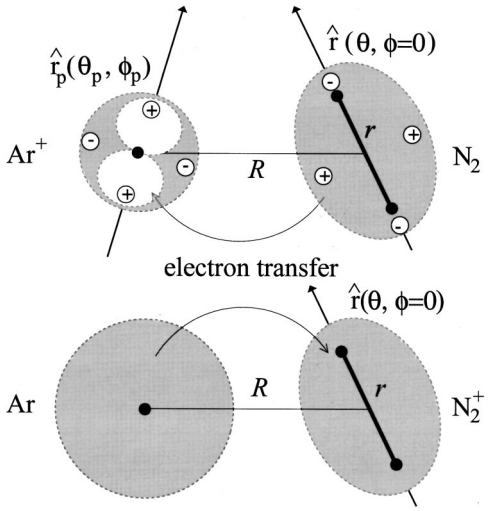

FIG. 1. Illustration of the relevant quantities in $Ar^+ + N_2$ and $Ar + N_2^+$ interactions. Signs refer to the quadrupole moments.

$$Ar^+(^2P_{3/2,1/2}) + N_2(X\,^1\Sigma_g^+), \qquad \text{(i)}$$

$$Ar^+(^2P_{3/2,3/2}) + N_2(X\,^1\Sigma_g^+), \qquad \text{(ii)}$$

$$Ar^+(^2P_{1/2,1/2}) + N_2(X\,^1\Sigma_g^+), \qquad \text{(iii)}$$

where the symbol $^2P_{j,\Omega}$ denotes the fine-structure levels of the ion in the electric field due to the weak intermolecular potential. Here Ω is the projection of the total electronic angular momentum j of Ar^+ along the intermolecular axis. States (i) and (ii) become degenerate at infinite intermolecular distance where they are separated from the state (iii) by the Ar^+ spin–orbit splitting. We build the interaction potential in the following sequence: dispersion, induction and electrostatic components are taken into account first and are combined with size effects defining the repulsion; charge exchange and spin–orbit couplings are then included. This approach emphasizes the role of the various interaction components in defining the main features of the potential energy surfaces.

To represent the potential of the Ar^+ ion interacting with the N_2 molecule we use a body-fixed expansion,[35]

$$V(R,\theta,\theta_p,\phi_p) = \sum_{a,\alpha} U_{a\alpha}(R,\theta) Y_{a\alpha}(\theta_p,\phi_p), \tag{2}$$

and

$$U_{a\alpha}(R,\theta) = \sum_{b} U_{ab\alpha}(R) Y_{b-\alpha}(\theta,0), \tag{3}$$

where $Y_{\ell m}$ are spherical harmonics[36] and the radial coefficients $U_{ab\alpha}$ have to be determined. The polar angles θ_p and ϕ_p specify the orientation of the half-filled p-orbital axis with respect to a body-fixed frame: we take **R** to lie along the z axis and **r** to lie on the xz plane (see Fig. 1). Only the θ angle is necessary to specify the orientation of the N_2 molecule in this frame. Because the homonuclearity of N_2 only even values of b occur in the sum in Eq. (3). The expansion

in Eq. (2) is analogous to that used to describe the collision of an atom in a P state with a closed-shell atom,[37,38] the difference being the dependence of the quantities $U_{a\alpha}$ on the molecular orientation. The diabatic potential energy surfaces defining the reactant states are elements of the interaction potential in Eq. (2) in an electronic diabatic basis. There are different bases (coupling schemes of angular momentum) which could be used.[37] In this case, we have found it convenient to choose the coupled basis set $|j\Omega\rangle$. In this representation, the interaction potential has both diagonal $\langle j\Omega|V|j\Omega\rangle$ and off-diagonal $\langle j\Omega|V|j'\Omega'\rangle$ matrix elements.

We obtain a 3×3 Hermitian interaction matrix,

$$\mathbf{U}=U_{00}\mathbf{1}+\frac{1}{5}\begin{pmatrix} 0 & (2/\sqrt{3})U_{22} & -\sqrt{2}U_{20} \\ (2/\sqrt{3})U_{22} & -U_{20} & \sqrt{2}U_{22} \\ -\sqrt{2}U_{20} & \sqrt{2}U_{22} & U_{20} \end{pmatrix} - \frac{i}{5}\begin{pmatrix} 0 & U_{21} & +\sqrt{3}U_{21} \\ -U_{21} & 0 & \sqrt{2}U_{21} \\ -\sqrt{3}U_{21} & -\sqrt{2}U_{21} & 0 \end{pmatrix}, \tag{4}$$

where only the $a=0$ ($\alpha=0$) and $a=2$ ($\alpha=-2,1,0,1,2$) terms contribute, and we have made use of the relation $U_{a\alpha}=(-)^{\alpha}U_{a-\alpha}$. The approach of $Ar^+(^2P)$ to the N_2 molecule gives rise to three doublet adiabatic potentials, i.e., the eigenvalues of matrix $\mathbf{U}$ in Eq. (4), namely, $1\,^2A'$, $2\,^2A'$, and $1\,^2A''$ in the C_s symmetry. These electronic states of the $(Ar–N_2)^+$ complex correlate to the $^2\Sigma^+$ and to the doubly degenerate $^2\Pi$ states in the linear configuration ($C_{\infty v}$ symmetry) and to the $^2A_1$, $^2B_2$, and $^2B_1$ states for perpendicular geometries (C_{2v} symmetry). At infinite intermolecular distance these potentials have the same energy and correlate to $Ar^+(^2P)+N_2$. The explicit expressions for the lowest order anisotropic functions $U_{a\alpha}$ are obtained from Eq. (3),

$$\begin{aligned} U_{00}(R,\theta)&=U_{000}(R)+U_{020}(R)Y_{20}(\theta,0), \\ U_{20}(R,\theta)&=U_{200}(R)+U_{220}(R)Y_{20}(\theta,0), \\ U_{21}(R,\theta)&=U_{221}(R)Y_{2-1}(\theta,0), \\ U_{22}(R,\theta)&=U_{222}(R)Y_{2-2}(\theta,0), \end{aligned} \tag{5}$$

where only the terms corresponding to $b=0$ and $b=2$ have been included in the sum. Once the radial body fixed coefficients, $U_{ab\alpha}(R)$, are known, the potential energy surfaces can be easily computed by inserting Eq. (5) into Eq. (4). In order to determine the $U_{ab\alpha}(R)$ coefficients [see Eqs. (2) and (3)] we exploit their relationship[35] with the radial coefficients $V_{abc}(R)$ occurring in the space-fixed expansion of the interaction potential,

$$U_{ab\alpha}(R)=\sum_c \langle a\alpha b-\alpha|c0\rangle V_{abc}(R), \tag{6}$$

where $\langle\cdots|\cdots\rangle$ is a Clebsch–Gordan coefficient[36] and $0\leqslant c\leqslant(a+b)$ (in the present case $c=0,2,4$). A brief discussion about the role and nature of each radial coefficient $V_{abc}(R)$ will be presented in the following section, while their parameterization will be given in the Appendix.

Concerning the exit channels, asymptotically they converge to

$$Ar+N_2^+(X\,^2\Sigma^+_{g,1/2}), \qquad \text{(iv)}$$

$$Ar+N_2^+(A\,^2\Pi_{u,1/2}), \qquad \text{(v)}$$

$$Ar+N_2^+(A\,^2\Pi_{u,3/2}). \qquad \text{(vi)}$$

Here $X\,^2\Sigma^+_{g,1/2}$, $A\,^2\Pi_{u,1/2}$, and $A\,^2\Pi_{u,3/2}$ are the electronic states of N_2^+ which can be formed in the charge transfer process. States (iv) and (v) are symmetric (A'), (vi) is antisymmetric (A'') with respect to a reflection in the triatomic complex plane; states (v) and (vi) are separated by spin–orbit splitting as $R\to\infty$. However state (vi) is weakly coupled, by charge exchange, to the reactant electronic states (i)–(iii) because of the small overlap of the orbitals which describe the electron after and before the jump (see below and also Refs. 22, 23, 25). Therefore it seems reasonable to consider only channels (iv) and (v). The diabatic potential energy surfaces of the Ar atom interacting with the N_2^+ molecular ion in both the $X(A')$ and $A(A')$ electronic states are expanded in Legendre polynomials,

$$V_X(R,\theta)=V_0^X(R)+V_2^X(R)P_2(\cos\theta), \tag{7}$$

and

$$V_A(R,\theta)=V_0^A(R)+V_2^A(R)P_2(\cos\theta), \tag{8}$$

where $V_X(R,\theta)$ and $V_A(R,\theta)$ refer to the exit channels (iv) and (v), respectively. Our analysis does not include the coupling between states (iv) and (v). Also, we take $V_A(R,\theta)=V_X(R,\theta)+\varepsilon$, where ε is the spectroscopic separation between the two asymptotic states ($\varepsilon=1.135$ eV). With these assumptions, the expansions in Eqs. (7) and (8) are equivalent to that typically used to represent the interaction of an atom in an S state with a structureless diatomic molecule. The nature and parameterization of V_0^X and V_2^X are discussed in Sec. IV C.

As stressed earlier, a crucial interaction component in the $(ArN_2)^+$ system is the coupling between the reactant and product channels by charge exchange. As emphasized in Refs. 22 and 25, only the charge transfer integrals J_σ and J_π, which involve respectively the overlap of the p_z atomic orbital of Ar with the σ_g and π_u molecular orbitals of N_2, play a relevant role. These integrals give an important contribution to the coupling of each of the states (i)–(iii) with the charge transfer states (iv) and (v). Accordingly, in the determination of the Hamiltonian matrix elements (see below) we take into account only J_σ and J_π. The dependence of the charge transfer integrals on the nuclear geometry of the complex $(ArN_2)^+$ and on the intermolecular distance R is again discussed in the next section and in the Appendix.

We must also include the spin–orbit interaction in Ar^+ which gives rise to the splitting of the reactant asymptote into the fine structure states (i)–(iii). The spin–orbit Hamiltonian of the atomic ion is assumed to be independent of R,[39]

$$\mathbf{V}_{so}=-(2/3)\,\delta\mathbf{L}\cdot\mathbf{S}, \tag{9}$$

where **L** and **S** are the electronic and spin angular momentum operators, respectively, and δ is the Ar^+ spin–orbit constant ($\delta = 0.178$ eV). In the coupled basis $|j\Omega\rangle$ the resultant matrix is diagonal, with elements $\langle j\Omega|\mathbf{V_{so}}|j\Omega\rangle = -\delta/3[j(j+1)-11/4]$. We add these constant energies to the diabatic potentials U_{11}, U_{22}, and U_{33}, which are the diagonal elements of the matrix **U** in Eq. (4) for all nuclear configurations.

The resultant 5×5 electronic Hamiltonian matrix H has the following form:

state	(i)	(ii)	(iii)	(iv)	(v)
(i)	$\mathsf{U}_{11}+2\delta/3+\Delta$	U_{12}	U_{13}	$-\mathsf{J}_G/(3)^{1/2}$	$-\mathsf{J}_\pi/(3)^{1/2}$
(ii)	U_{21}	$\mathsf{U}_{22}-\delta/3+\Delta$	U_{23}	0	0
(iii)	U_{31}	U_{32}	$\mathsf{U}_{33}-\delta/3+\Delta$	$(2/3)^{1/2}\mathsf{J}_\sigma$	$(2/3)^{1/2}\mathsf{J}_\pi$
(iv)	$-\mathsf{J}_\sigma/(3)^{1/2}$	0	$(2/3)^{1/2}\mathsf{J}_\sigma$	V_X	0
(v)	$-\mathsf{J}_\pi/(3)^{1/2}$	0	$(2/3)^{1/2}\mathsf{J}_\pi$	0	$V_X+\varepsilon$,

(10)

where the constant Δ denotes the asymptotic energy difference between $Ar^+(^2P)$ and N_2^+ ($\Delta = 0.238$ eV) and zero energy corresponds to V_X at $R=\infty$ [see Eq. (7) and the asymptote channel (iv)]. The present potentials have no explicit dependence on N_2 and N_2^+ bond distances; the weak dependence of each radial coefficient upon the internuclear distance r and the relatively small change in the equilibrium and in the vibrational frequency, passing from $N_2(X\,^1\Sigma_g^+)$ to $N_2^+(X\,^2\Sigma_g^+)$ and $N_2^+(A\,^2\Pi_u)$, justify the assumption of no explicit dependence of H from r.[25] The five lowest electronically adiabatic potential energy surfaces $\mathsf{E}_i(R,\theta)$ are just the eigenvalues of the matrix H. At infinite intermolecular distance they correlate, in order of increasing energy, to the electronic states (iv), (i)–(iii), and (v). For state (v) we neglect spin–orbit coupling since this channel is not accessible at the low collision energies considered in the present study.

B. Radial coefficients for the $Ar^+ + N_2$ channel

An important aspect of our analysis is the identification of the proper correspondence between the radial coefficients V_{abc} in Eq. (6) and the different components (dispersion, induction, electrostatic, repulsion, etc.) of the total interaction. Such correspondence permits us to determine the strength and dependence upon R of the V_{abc} coefficients by making use of correlation formulas[30–34] which are based on information extracted from scattering experiments in combination with other data (details are reported in the Appendix). These correlation formulas provide the main features of each interaction component in terms of fundamental physical properties of the interacting partners, such as polarizability, charge, and quadrupole moment. Here a brief discussion of the role and nature of each radial coefficient in Eq. (6) for the $Ar^+ + N_2$ system is presented.

The leading $V_{000}(R)$ term describes the spherical interaction of van der Waals nature, i.e., the interaction averaged over all the possible orientations of the two partners. This component arises from a proper combination of the short range repulsion, due to the average size of the interacting partners, with a long range attraction associated with the average induction and dispersion forces. Its main features depend on the polarizability and charge of the partners.[30–32]

The V_{022} term represents the interaction anisotropy associated with different alignments of the half-filled orbital of the open-shell ion. In particular, it accounts for changes in the repulsion, in the dispersion and in the induction energies. Estimates, performed following Ref. 40, suggest that here the effect of the V_{022} term is negligible. The most important contribution, determined by the variation of the open shell ion alignment, is the change in the charge transfer integral J_σ and J_π [the basic off-diagonal term in the Hamiltonian matrix, see Eq. (10)], which we discuss later.

The V_{202} term describes the effect of the molecular anisotropy on the interaction with a spherical ion. This term incorporates the effect of the molecular size, dominant at short range and dependent on the molecular polarizability anisotropy, of the induction (ion-induced multipole) and of the electrostatic forces (ion–molecular quadrupole) prevailing at long range.

The V_{220}, V_{222}, and V_{224} coefficients emphasize the role of the anisotropy arising from the relative orientation of the half-filled orbital of the ion and the nitrogen molecular axis. The most relevant effects are ascribed to V_{224} which represents the quadrupole–quadrupole interaction, while V_{220} and V_{222} are corrective terms which together contribute to define the global size of the system.[29]

C. Radial coefficients for the $Ar + N_2^+$ channel

In the case of the interaction of a molecular ion with a closed shell atom the radial coefficients [see Eqs. (7) and (8)] have a direct physical meaning. The isotropic $V_0^X(R)$ term arises from the combination of an average repulsion, due to the size of the two partners, with an average attraction that arises from the isotropic induction and dispersion forces. The anisotropic $V_2^X(R)$ component is exclusively determined by the combination of the anisotropy in the size of molecular ion with that in the dispersion attraction.

The main features of the $V_0^X(R)$ and $V_2^X(R)$ components have been derived using an extension[34] of our empirical methods,[30–33] recently introduced to evaluate an anisotropic

TABLE I. Parameters of the radial coefficients.

		Ar^+-N_2	N_2^+-Ar
V_{000}	R_m (Å)	3.13	
	ϵ (meV)	120	
	β	5.50	
	C_4 (meV Å^4)	1.62×10^4	
	R_1 (Å)	3.44	
	R_2 (Å)	4.85	
	b_1	−0.8210	
	b_2	1.2823	
	b_3	−3.1168	
	b_4	3.7032	
V_{202}	A_{202} (meV)	2.10×10^6	
	α_{202} (Å^{-1})	3.30	
	C_{202} (meV Å^4)	6.14×10^3	
	B_{202} (meV Å^3)	-4.44×10^3	
V_{224}	C_{224} (meV Å^5)	-3.61×10^3	
V_0^X	R_m (Å)		3.49
	ϵ (meV)		89.6
	β		5.50
	C_4 (meV Å^4)		1.83×10^4
	R_1 (Å)		3.84
	R_2 (Å)		5.41
	b_1		−0.8210
	b_2		1.2941
	b_3		−3.0907
	b_4		3.5197
V_2^X	A_2 (meV)		5.50×10^6
	α_2 (Å^{-1})		3.30
	C_2 (meV Å^6)		1.29×10^4

atom–molecule interaction potential. $V_0^A(R)$ and $V_2^A(R)$ are taken to coincide with $V_0^X(R)$ and $V_2^X(R)$, respectively.

D. The charge transfer couplings

It is well known that the charge exchange integrals J_σ and J_π decrease exponentially with the intermolecular distance, in accordance with the behavior of the overlap integral related to the transferred electron.[25,41–44] The radial dependence and strength of the couplings are due to the ionization potential of the donor and the electronic affinity of the acceptor (here the ionization potentials of N_2 and Ar both play an important role), and to the polarizability and charge of the particles, and have been calculated following Ref. 33. On the basis of the angular dependence of the overlap integral between orbitals which describe the electron before and after the jump, we assign the maximum value of J_σ at $\theta=0$, while it decreases as θ tends to $\pi/2$. J_π is zero for $\theta=0$ and increases towards its maximum value at $\theta=\pi/2$ (see Appendix). The main features of J_σ and J_π agree with results previously computed.[22]

III. POTENTIAL ENERGY SURFACES

The interaction has been calculated, using the radial coefficients given in the Appendix and the parameters of Table I, at increasing levels of complexity. First, J_σ, J_π, and δ in Eq. (10) have been set to zero to emphasize the effects of the dispersion, induction, and electrostatic forces combined with the repulsion due to the size of the outer electronic orbitals. Results for parallel and perpendicular configurations are plotted in Fig. 2. In such a case the interaction anisotropy is mainly dominated by the angular modulation of the repulsion, quadrupole–quadrupole, and ion–quadrupole interactions while dispersion and induction play a minor role. Then all terms in Eq. (10) have been considered and a full diagonalization provides the five lowest adiabatic potential energy surfaces, whose cuts at $\theta=0$ and $\theta=\pi/2$ are plotted as functions of R in Fig. 3. Comparison with Fig. 2 permits a direct assessment of the basic contribution of the charge exchange component (J_σ, J_π) to the stabilization of the complex. The dependence of the interaction on the angular variable, θ, is reported in Fig. 4 for the ground and excited potential energy surfaces. Here the intermolecular distance has been fixed at 2.70 Å, which represents the equilibrium distance of the complex in the ground electronic state, to allow a proper comparison with recent and accurate theoretical results from Landenberg *et al.*[45] Good agreement is found both in the strength and in the angular dependence of the interaction. In

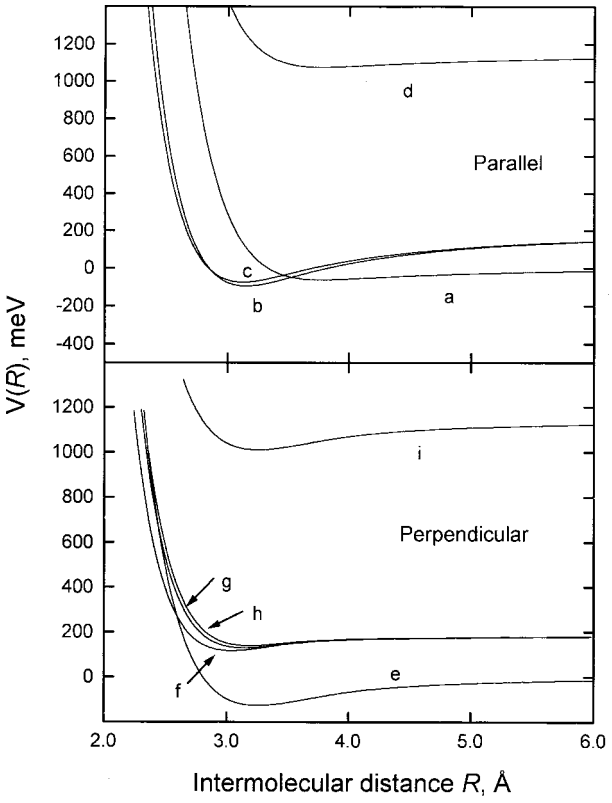

FIG. 2. Curves, corresponding to cuts of the potential energy surfaces generated from Eq. (10) putting spin–orbit splitting and charge transfer integrals equal to zero, are plotted to emphasize the selective role of the interaction components (see text) and to show the correlation between the asymptotic levels and the molecular states of the complex. Parallel geometry: (b) and (c) correlate the $Ar^+(^2P)+N_2$ asymptote, respectively, with the $^2\Sigma(^2A')$ and the $^2\Pi(^2A', ^2A'')$ molecular states (corresponding states of the C_s group are in parentheses), while (a) and (d) connect the $Ar+N_2^+(^2\Sigma_g^+, ^2\Pi_u)$ asymptotes, respectively, with the $^2\Sigma(^2A')$, and the $^2\Pi(^2A')$ molecular states. Perpendicular geometry: (f), (g), and (h) correlate the $Ar^+(^2P)+N_2$ asymptote respectively, with the $^2B_2(^2A')$, $^2B_1(A'')$, and $^2A_1(^2A')$ molecular states (corresponding states of the C_s group are again in parentheses), while (e) and (i) connect the $Ar+N_2^+(^2\Sigma_g^+, ^2\Pi_u)$ asymptotes, respectively, with two $^2A_1(^2A')$ molecular states.

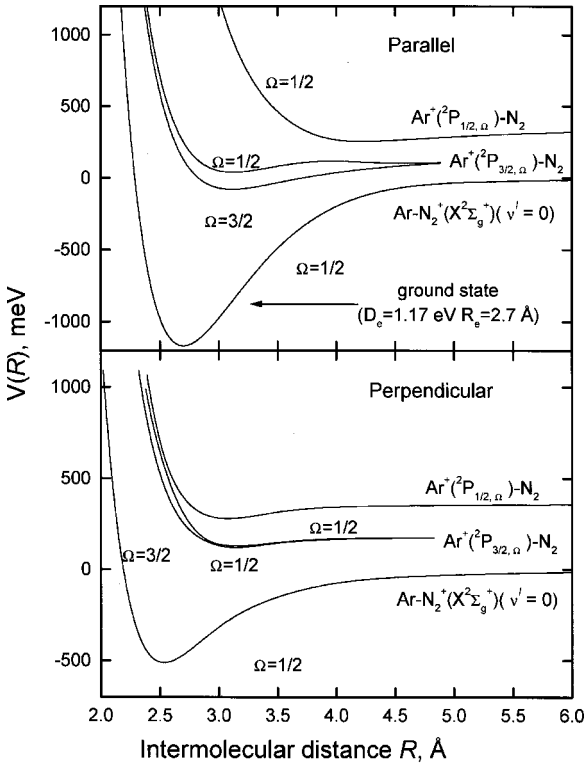

FIG. 3. Adiabatic potential curves in the parallel and perpendicular geometries, labeled in terms of $\Omega=3/2$ and $\Omega=1/2$ asymptotic states. The excited potential, leading to $Ar+N_2^+$ $(A\ ^2\Pi_u)$, is not plotted.

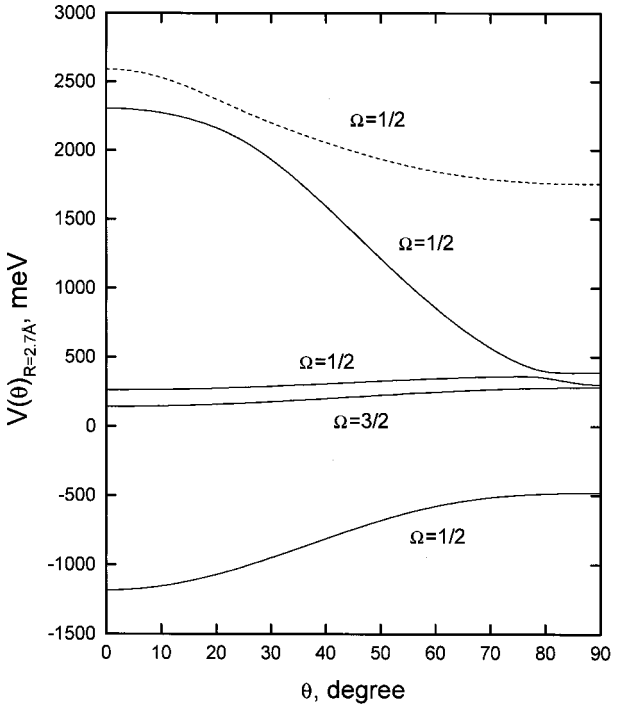

FIG. 4. θ dependence (see Fig. 1) of the potential energy surfaces, labeled in terms of Ω. The dashed line refers to the excited surface asymptotically correlating with $Ar+N_2^+$ $(A\ ^2\Pi_u)$. In all cases the intermolecular distance has fixed at $R=2.70$ Å.

addition, the bond energy predicted for the $(Ar–N_2)^+$ linear complex (1.17 eV) is very close to the experimental value (1.09 eV).[46]

Vibronic surfaces: Experimental findings show that charge transfer processes in the $(Ar–N_2)^+$ system occur with high efficiency via simultaneous vibrational and electronic (hence vibronic) transitions. In the present work we follow the suggestion of Nikitin and co-workers.[25] These authors have shown that for the $(Ar–N_2)^+$ system the vibronic states $\mathsf{E}_i^{\nu}(R,\theta)$ can be expressed as

$$\mathsf{E}_i^{\nu}(R,\theta)=\mathsf{E}_i(R,\theta)+\mathsf{E}_{\nu}, \tag{11}$$

where E_{ν} are the solutions for the vibrational contribution alone and depend, in principle, on both the vibrational energies of N_2 and N_2^+. The adiabatic vibronic curves, defining the entrance $Ar^+(^2P_{3/2,1/2})+N_2(X\ ^1\Sigma_g^+)(\nu=0)$ and the exit $Ar+N_2^+(X\ ^2\Sigma_g^+)(\nu')$ channels are expected to exhibit, according also to Bauer, Fischer, and Gilmore,[47] values of E_{ν} close to those of $N_2^+(\nu')$ ($\mathsf{E}_{\nu'=0}$ is here assumed to be equal to zero). In Ref. 25, some information is provided on the coupling at the crossings, and it is suggested that transition probabilities can be properly calculated within the Landau Zener model.

The nonadiabatic coupling between vibronic states is introduced as a perturbation at the crossings.[25,48] Such couplings are small (of the order of tens of meV) implying that nonadiabatic transitions are localized near the crossings. Our analysis assumes crossings between the entrance channel $Ar^+(^2P_{3/2,3/2})+N_2(X^1\Sigma_g^+)(\nu=0)$ and $Ar+N_2^+(X^2\Sigma_g^+)(\nu')$ exit channels to be fully diabatic because the nonadiabatic coupling terms are expected to be very small. This behavior can be ascribed to the reduced role of charge transfer effects determined by the symmetry property of the system in the entrance (ii) and exit (iv) and (v) channels. Crossings, considered relevant for the present dynamical calculations, are shown in Fig. 5.

IV. DYNAMICS OF THE CHARGE-TRANSFER PROCESS

At the low collision energies considered in the present work ($E\leqslant 2$ eV), the formation of N_2^+ products in the first excited electronic state $A\ ^2\Pi_u$ can be neglected, although the influence of such a state on the features of low lying potential energy surfaces has to be considered (see Sec. II). In the present study we find it convenient to describe the charge transfer process by calculating the total probability $P_{j\nu'}(E,\theta)$ for the formation of $N_2^+(X\ ^2\Sigma_g^+)$ in a particular vibrational state ν' considering the reactant $Ar^+(^2P_j)$ in the fine structure level j and $N_2(X\ ^1\Sigma_g^+)(\nu=0)$ at a fixed θ (see Fig. 1). The calculation has been performed for arbitrary l, the quantum number representing the orbital angular momentum of the collision complex, which classically corresponds to a specific impact parameter b,

$$b=\frac{(l(l+1))^{1/2}}{k}, \tag{12}$$

where k is the wave number defined as $k=\mu v_{\mathrm{rel}}/\hbar$, μ is the reduced mass of the system, and v_{rel} is the relative velocity of the colliding partners. Such a procedure considers nona-

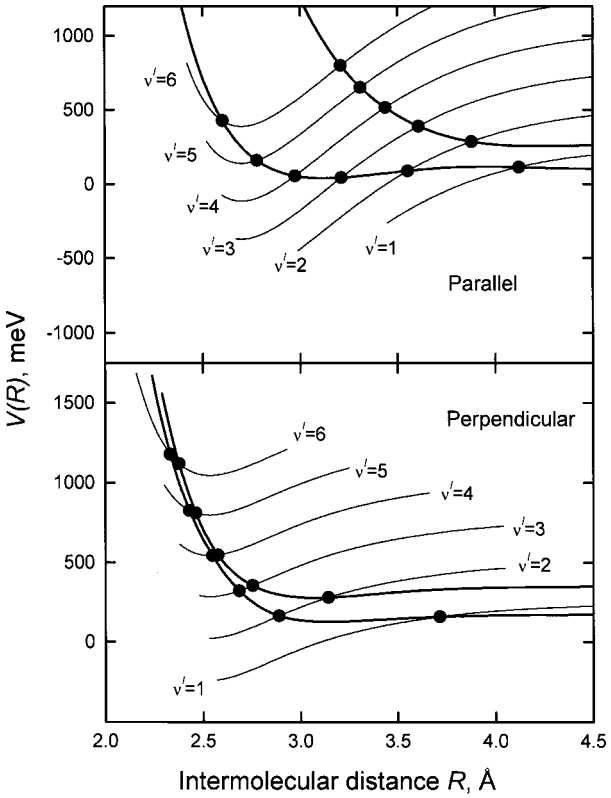

FIG. 5. Sequence of crossings between the potential curves ($\Omega=1/2$) correlating the entrance channels $Ar^+(^2P_{3/2,1/2})+N_2(X\,^1\Sigma_g^+)(\nu=0)$ and $Ar^+(^2P_{1/2,1/2})+N_2(X\,^1\Sigma_g^+)(\nu=0)$ (see Fig. 3) with the exit channels $Ar+N_2^+(X\,^2\Sigma_g^+)(\nu')$. The latter are obtained as discussed in Sec. III A.

diabatic events at crossings to be independent and neglects interference effects. $P_{j\nu'}(E,\theta,l)$ is therefore obtained as a proper combination of p_x, the probability of diabatic passage through the xth curve crossing (see Fig. 5). At the low collision energies considered, it can be represented[49–51] as

$$p_x(E,\theta,l)=\exp\left(-\frac{2\pi H(R_x,\theta)^2}{\hbar v_R \Delta_x}\right), \tag{13}$$

where R_x is the intermolecular distance at the crossing, Δ_x defines the absolute difference of the slope of the potential curves, and $H(R_x,\theta)$ corresponds to the matrix element of the nonadiabatic coupling, whose role will be discussed later. The radial velocity v_R at the same crossing is given by

$$v_R^2=\frac{2}{\mu}\left[E\left(1-\frac{l(l+1)}{k^2R_x^2}\right)-E_x\right], \tag{14}$$

where E_x represents the value of the potential energy at the crossing. It should be noted that E_x, R_x, and Δ_x vary with θ according to the properties of the interaction potential energy surfaces (see Sec. III and Fig. 5).[52] The charge transfer total cross section $\sigma_{j\nu'}(E,\theta)$, may be written as a sum of contributions from each l,

$$\sigma_{j\nu'}(E,\theta)=\frac{\pi}{k^2}\sum_{l=0}^{l_{\max}}(2l+1)P_{j\nu'}(E,\theta,l), \tag{15}$$

where

$$l_{\max}=kR_x\left(1-\frac{E_x}{E}\right)^{1/2}, \tag{16}$$

is the maximum value of l for which v_R is real [the corresponding $b_{\max}$ value is defined according to Eq. (12)]. In the dynamical studies of this paper the integral cross section, $\sigma_j(E)$, is obtained by averaging the $\sigma_{j\nu'}(E,\theta)$ calculated for the collinear and perpendicular configurations of the collision complex and summing the contributions for the various exit channels ν'. Finally, the integral average cross section $\sigma(E)$ is defined as

$$\sigma(E)=w_{3/2}\sigma_{3/2}(E)+w_{1/2}\sigma_{1/2}(E). \tag{17}$$

In the case of beam experiments performed with a statistical distribution of $Ar^+(^2P_j)$, the relative weights $w_{3/2}$ and $w_{1/2}$ become equal, respectively, to 2/3 and 1/3. Moreover, the $w_{3/2}$ reduces to 1/3 when the $Ar^+(^2P_{3/2,3/2})+N_2(X\,^1\Sigma_g^+)(\nu=0)$ channel is considered not effective (see above).

V. THE NONADIABATIC COUPLING MATRIX ELEMENT

A key point to be investigated concerns the analysis of the role and nature of the nonadiabatic coupling matrix element H. As usual[47,53,54] this crucial quantity can be factorized as

$$H^2(R,\theta,\nu)=\mathcal{H}^2(R)f(\theta)q(\nu,\nu'), \tag{18}$$

where $\mathcal{H}(R)$ depends on the electron exchange and is expected to decrease exponentially with the intermolecular separation,[54] $f(\theta)$ describes the angular dependence of the coupling, and $q(\nu,\nu')$ is the Franck–Condon factor (FCV) for the transition $\nu-\nu'$.[55]

The factor is introduced to account for the different time scale of the charge transfer process with respect to that typical of the vibrational motion. However, very often this results in a negligible probability for the formation of vibrationally excited products, at odds with experimental observations. It has therefore been proposed[21,28] that the above expression must be used only at high collision energies when the non-adiabatic process can be safely considered almost instantaneous (a vertical transition), whereas for slow collisions H must be represented in a different way. In other words, when the transition duration is comparable with or longer than the vibrational period, the FC picture is no longer valid and Eq. (18) becomes

$$H^2(R,\theta)=\mathcal{H}^2(R)f(\theta). \tag{19}$$

Indeed, experiments performed at collision energies below 1 eV (Refs. 4, 10) have clearly indicated the formation of $N_2^+(X\,^2\Sigma_g^+)$ in excited vibrational states up to $\nu'=4$, although the corresponding FC factors are negligible.

We have performed extensive preliminary calculations, by using Eq. (19) and considering the $Ar^+(^2P_{3/2})+N_2(X\,^1\Sigma_g^+)$ and $Ar^+(^2P_{1/2})+N_2(X\,^1\Sigma_g^+)$ entrance channels both with statistical weights 1/3, to assess the sensitivity of the cross section $\sigma(E)$ to the strength of the coupling matrix element H. Results reported in Fig. 6 show clearly that the steplike behavior corresponds to the successive

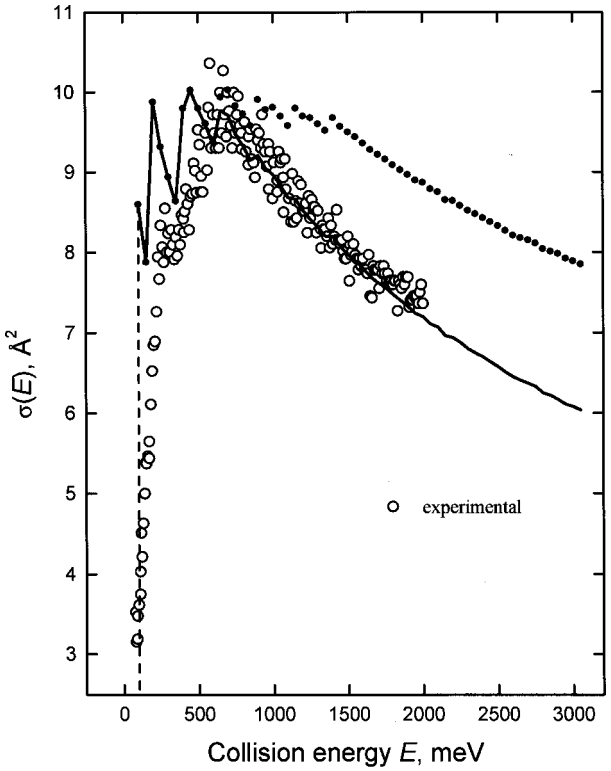

FIG. 6. Comparison between cross sections, $\sigma(E)$, calculated according to the present analysis, and experimental data of Ref. 1 increased, within the experimental uncertainty, of ~20%. Dashed line represents the thermodynamic threshold of the product $N_2^+(X\,^2\Sigma_g^+)(\nu'=1)$. Dotted line describes results of a typical Landau–Zener treatment, without time restriction, and solid line refers to the analysis which uses a time limitation in the collision dynamics defined in terms of a particular $\tau_{\min}$ sequence (see text).

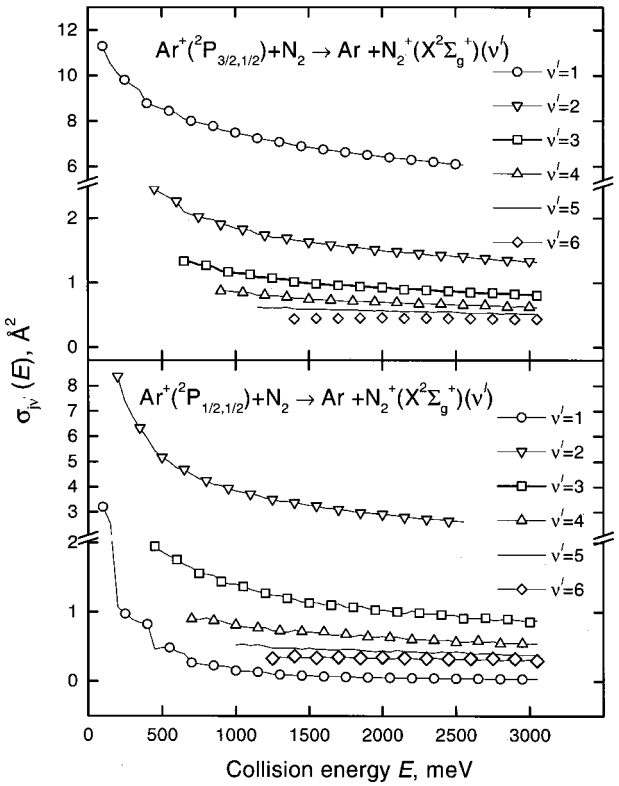

FIG. 7. Individual contributions $\sigma_{j\nu'}(E)$ to the cross section $\sigma(E)$ (see dashed line in Fig. 6), calculated as a function of the collision energy E. The different appearances account also for the change in the thermodynamic thresholds.

opening of the various exit channels $Ar+N_2^+(X\,^2\Sigma_g^+)(\nu')$ and confirm that the strength of the coupling matrix element H must be of the order of ~10 meV to obtain cross sections $\sigma(E)$ in the region of tens of Å^2, in agreement with experimental results reported in Ref. 1 (see also Refs. 2, 7). The comparison between experimental and calculated values shows that position and value of the cross section maximum are well reproduced, however marked discrepancies appear in the energy dependence of $\sigma(E)$ (see dotted line in Fig. 6).

For a more complete analysis, we have found it necessary to deal separately with the contributions of the various exit channels $\sigma_{j\nu'}$ (see Fig. 7). Calculations suggest that the main products are $N_2^+(X\,^2\Sigma_g^+)(\nu'=1)$ and $N_2^+(X\,^2\Sigma_g^+)(\nu'=2)$, in agreement with experimental findings.[7] However, also $N_2^+(X\,^2\Sigma_g^+)(\nu'=3,4)$ are formed with an appreciable cross section which decreases slowly with the collision energy. This contrasts with experimental findings:[4,10] $N_2^+(X\,^2\Sigma_g^+,\nu'=3,4)$ have been exclusively observed within a narrow range of E values. In addition, $\sigma_{3/2}(E)$ and $\sigma_{1/2}(E)$ appear to be quite similar and this also contradicts experimental observations.[7,8,17]

Further progress can be achieved by using a more complete representation of the nonadiabatic coupling term H, including explicitly the dependence upon the vibrational states of reactants and products. As already stressed, the charge transfer reaction investigated here is not a simple FC process and therefore its description requires a proper assessment of the role of molecular vibration in both the entrance and exit channels. We suggest to use, as a general criterion, the condition that the time required for molecular rearrangement must be matched to the duration of the transition at vibronic crossings. Bobashev and Kharchenko[56] have proposed the following expression for the time τ associated with a nonadiabatic transition at the xth crossing:

$$\tau=\left[\left(\frac{\hbar}{2v_R\Delta_x}\right)^2+\left(\frac{H(R_x,\theta)}{v_R\Delta_x}\right)^4\right]^{1/4}, \tag{20}$$

where H includes only electronic contributions [see Eq. (19)].

The transition time depends on two different contributions: the first, dominant when the H term is small and the product $v_R\Delta_x$ is sufficiently large, describes the diabatic limiting case. The second is important in the opposite situation and describes the limiting adiabatic case. Both contributions vary with the radial velocity v_R and thus τ depends both on the collision energy and on the impact parameter. This means that for each value of the collision energy, the achievement of time matching depends critically on the impact parameter, or the angular momentum in a fully quantum approach (a similar dynamical treatment has been successfully applied to the investigation of the "harpooning," mechanism in some chemiluminescent reactions of the excited calcium atom[57]).

We therefore suggest that the coupling H, at the xth crossing, must be represented as in Eq. (18) for collisions occurring at $b \leqslant b_{\min}$, where $b_{\min}$ is the impact parameter for which the transition time τ [see Eq. (20)] is equal to a critical

value, τ_{min} so that transitions with $\tau < \tau_{min}$ can be considered to be instantaneous with respect to the period of molecular vibration. In contrast, collisions with $b > b_{min}$ induce transitions which are sufficiently slow with respect to the molecular vibrations. Under such condition, H is expected to include only electronic contributions, see Eq. (19).

Numerical experiments have been performed using different sequences of τ_{min} values, always on the femtosecond scale, corresponding to variable fractions of the molecular vibration period of N_2 and N_2^+ ($\sim$10 fs). In any sequence the τ_{min} parameter has been assumed to increase with the $(\nu' - \nu)$ difference, as suggested by the occurrence of a more pronounced molecular rearrangement.

Calculations with $\tau_{min} > 1.0$ fs show a sharper decrease of $\sigma(E)$ at high energies respect to results of a Landau–Zener treatment without time restrictions. To understand the origin of this behavior it must be noted that the formation of $N_2^+(X\,^2\Sigma_g^+)$ in specific ν' levels mainly arise here from collisions which probe different intervals $b_{max} - b_{min}$ [contributions from $b < b_{min}$ are damped by the FC factors, see Eqs. (13) and (18)], leading therefore to scattering of the products at specific angles. Such intervals of impact parameters, which we shall refer as ''windows,'' vary with the collision energy E, so that the levels $\nu' = 3$ and $\nu' = 4$ tend to be produced exclusively in a particular energy range, in accordance with experimental findings.[4,10]

VI. FURTHER COMPARISON WITH EXPERIMENTS

Integral cross sections $\sigma(E)$, calculated according to the procedure discussed above and using a specific sequence of τ_{min} (τ_{min} increases linearly from 3.0 to 4.0 fs as ν' changes from $\nu' = 1$ to $\nu' = 6$), are compared in Fig. 6 with experimental data.[1] Calculated $\sigma(E)$ are in satisfactory agreement, in the 0.1–2 eV collision energy range, with experimental results. The present analysis confirms that the steplike behavior in $\sigma(E)$ is due to the successive opening of vibronic levels in the exit channels. In addition, the sharp decrease of σ after the maximum, which corresponds to a nontypical Landau–Zener behavior, can be ascribed to the progressive narrowing of the impact parameter windows, $b_{max} - b_{min}$, which mainly contribute to the formation of products in specific vibrational levels. As discussed in the previous section, these windows become particularly critical for the production of $N_2^+(X\,^2\Sigma_g^+)$ in $\nu' \geqslant 3$.

Another interesting comparison can be carried out between the calculated $\sigma_{1/2}/\sigma_{3/2}$ ratio and the experimental determination.[7,8,17] In agreement with the experimental findings, this study predicts a ratio smaller than 1.0, specifically $\sim$0.5, as shown in panel A of Fig. 8. This ratio decreases slightly with the collision energy E, again as experimentally observed.[7] Panel B of Fig. 8 shows the ratio between $\sigma_{3/2}(\nu' = 2)$ and $\sigma_{3/2}(\nu' = 1)$; predicted values are in the range found by Liao *et al.*[7]

VII. CONCLUSIONS

The present study provides an accurate description of the low-lying potential energy surfaces in the $(ArN_2)^+$ system. In the diabatic representation, the potential in the entrance and exit channels has been given as an expansion in spherical harmonics whose radial coefficients have been related to specific components of the interaction. Such components have been estimated by correlation formulas,[30–33] based on fundamental properties of the interacting partners such as polarizability, charge, quadrupole moment, ionization potential, and electron affinity. Adiabatic PES are obtained by diagonalizing the full Hamiltonian matrix [Eq. (10)] obtained by introducing into the diabatic representation of the interaction the charge exchange couplings and the spin–orbit term. Vibronic surfaces are then generated as suggested by Nikitin and co-workers.[25] This approach permits a treatment of the dynamics as a sequence of independent nonadiabatic transitions at localized crossings where the couplings are small and the transition probability can be adequately calculated within the Landau–Zener model.

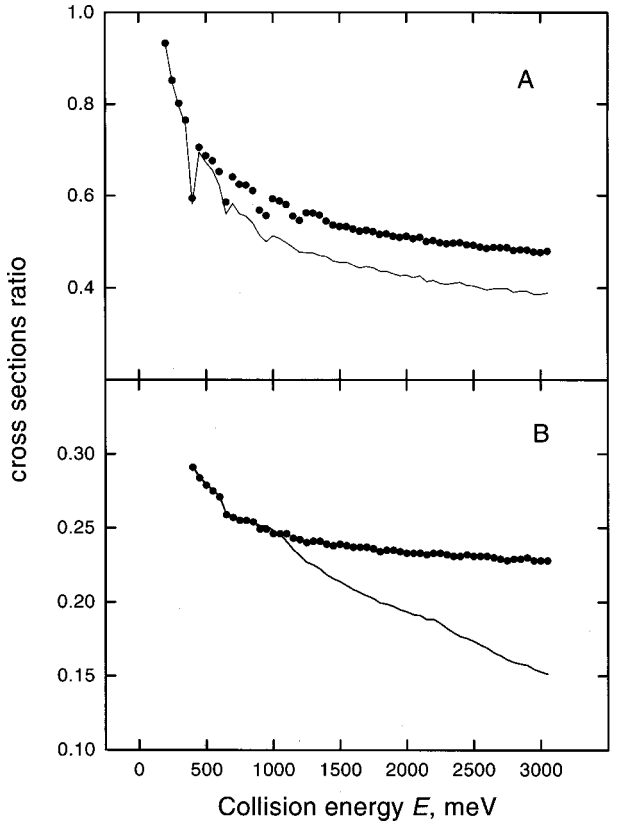

FIG. 8. Ratios $\sigma_{1/2}/\sigma_{3/2}$ (panel A) and $\sigma_{3/2}(\nu' = 2)/\sigma_{3/2}(\nu' = 1)$ (panel B) calculated as a function of collision energy E. In both panels dotted line and solid line as in Fig. 6.

The calculated ground PES provides the correct linear geometry of the $(ArN_2)^+$ complex and a value for its bond energy very close to the experimental determination.[46] Moreover, the full topography of the low lying PES is in good agreement with recent theoretical calculations.[45]

Particular attention has been addressed to the characterization of the transitions at a microscopic level. In our approach the collisional dynamics appears to be strongly affected by the requirement that the transition time τ, which depends on the collision velocity and impact parameter, has to match the time τ_{min} necessary for the molecular rearrangement into the final vibrational level. The system colliding at

high velocity and at small impact parameter falls in the limiting case of a vertical transition (or FC transition), which occurs suddenly with respect to the vibrational motion ($\tau < \tau_{min}$). Nonvertical transitions (or non-FC transitions) represent the opposite limiting case, involving large impact parameter and low velocity ($\tau > \tau_{min}$). The present approach leads to the identification of windows of impact parameters ($b_{max} - b_{min}$), where the formation of products in specific vibrational states becomes effective. As a consequence, N_2^+ ions in specific vibrational levels ν' are expected to be scattered into defined angular cones, as experimentally observed.[4,10] In addition, calculations of the integral cross section σ, carried out assuming a statistical distribution over the fine structure of the reagent $Ar^+(^2P_j)$, provide results in good agreement with the experimental data.[1]

In conclusion, the present analysis casts light on the origin of some findings observed in the $\sigma(E)$ behavior, such as the steplike ascent and the sharp decrease at higher energies. Finally, it predicts cross-section ratios for different entrance and exit channels that are in agreement with experimental evidence.[7,8,17]

APPENDIX: PARAMETERIZATION OF THE RADIAL COEFFICIENTS

$V_{000}(R)$, $V_0^X(R)$, and $V_0^A(R)$ have been represented by the usual Morse–Spline–van der Waals (MSV) parameterization.[32] Two boundary points R_1 and R_2 are chosen, and a Morse function is used for R values smaller than R_1,

$$f(R) = \epsilon\left\{ \exp\left[-2\beta\left(\frac{R}{R_m} - 1 \right) \right] - 2\exp\left[-\beta\left(\frac{R}{R_m} - 1 \right) \right] \right\}, \tag{A1}$$

while an R^{-4} ion-induced dipole dependence is employed for R values larger than R_2,

$$f(R) = -C_4 R^{-4}. \tag{A2}$$

The parameters ϵ and R_m represent the depth and the location of the well and have been calculated, on the basis of the polarizabilities of Ar^+,[32] N_2^+,[58] Ar,[31] and N_2,[59] by means of correlation formulas of Ref. 31. β is related to the curvature of the potential well, which is described by the Morse function, and has been fixed to the standard value for ion-neutral pair interaction.[32]

The C_4 term controls the attractive part of interaction. It is effectively a constant which includes the ion-induced dipole and dispersion contributions and can also be calculated from the polarizability and charge of the interacting partners.[31,32]

A cubic spline function,

$$f(R) = b_1 + \left(\frac{R}{R_m} - \frac{R_1}{R_m} \right) \left\{ b_2 + \left(\frac{R}{R_m} - \frac{R_2}{R_m} \right) \times \left[b_3 + \left(\frac{R}{R_m} - \frac{R_1}{R_m} \right) b_4 \right] \right\}, \tag{A3}$$

with coefficients b_i which insure the continuity of the potential and of the first derivatives at the match points R_1 and R_2, covers the range between R_1 and R_2. The choice of the match points does not affect appreciably the interaction energy.

For the present system V_{022} has been taken to be zero at all R (see text). V_{202}, V_2^X and V_2^A have been represented as

$$V_{202}(R) = A_{202}\exp(-\alpha_{202}R) - B_{202}R^{-3} - C_{202}R^{-4}, \tag{A4}$$

$$V_2^X(R); V_2^A(R) = A_2\exp(-\alpha_2 R) - C_2 R^{-6}, \tag{A5}$$

where B_{202} accounts for the ion–molecular quadrupole interaction. A_{202} and α_{202} describe the anisotropy of the short range repulsion and have been calculated following guidelines in Ref. 34. C_{202} and C_2 represent, respectively, the anisotropy in the ion-induced dipole and in the induced dipole-induced dipole attractions and have been calculated by considering the average value and anisotropy of the N_2 and N_2^+ polarizabilities.[58,59]

The V_{220} and V_{222} coefficients correspond to correction terms, and following suggestions given in Refs. 29, 60, have been represented as decreasing exponential functions of the type,

$$V_{abc}(R) = A_{abc}\exp(-\alpha_{abc}R). \tag{A6}$$

The parameters have been assumed to be related to those defining the exponential part of the term $V_{202}(R)$,

$$\alpha_{222} = \alpha_{220} = \alpha_{202},$$

$$A_{222} = -A_{220} = -A_{202}.$$

The quadrupole–quadrupole interaction term V_{224} takes the known analytical expression,

$$V_{224}(R) = C_{224}R^{-5}, \tag{A7}$$

where C_{224} depends on the quadrupole moment of the open-shell atom and of the diatomic molecule. For an ion with electronic configuration p^5, the quadrupole moment can be evaluated as $e\langle r_a^2\rangle$,[35] where e is the electron charge and r_a is the mean square radius of the outer orbitals. For the N_2 molecule, the value used has been taken from Ref. 61.

All the potential parameters are reported in Table I.

Finally the charge transfer integral J have been parameterized as

$$\mathrm{J}_\sigma(R,\theta) = J_0^{\sigma p_z}(R) + J_2^{\sigma p_z}(R)P_2(\cos\theta), \tag{A8}$$

and

$$\mathrm{J}_\pi(R,\theta) = J_2^{\pi_u p_z}(R)\sin^2\theta, \tag{A9}$$

where P_2 is a Legendre polynomial and the radial coefficients have been described as

$$J_0^{\sigma p_z}(R) = 78801R\exp(-2.028R), \tag{A10}$$

$$J_2^{\sigma p_z}(R) = 82762R\exp(-2.028R), \tag{A11}$$

$$J_2^{\pi_u p_z}(R) = 74841R\exp(-2.028R). \tag{A12}$$

[1] P. Tosi, O. Dmitrijev, and D. Bassi, Chem. Phys. Lett. **200**, 483 (1992).
[2] D. Smith and N. G. Adams, Phys. Rev. A **23**, 2327 (1981).
[3] W. Lindinger, F. Howorka, P. Lukac, S. Kuhn, H. Villinger, E. Alge, and H. Ramler, Phys. Rev. A **23**, 2319 (1981).

[4] A. L. Rockwood, S. L. Howard, W. H. Du, P. Tosi, W. Lindinger, and J. H. Futrell, Chem. Phys. Lett. **114**, 486 (1985).
[5] J. H. Futrell, Int. J. Quantum Chem. **31**, 133 (1987).
[6] S. L. Howard, Chem. Phys. Lett. **178**, 65 (1991).
[7] C.-L. Liao, J.-D. Shao, R. Xu, G. D. Flesch, Y.-G. Li, and C. Y. Ng, J. Chem. Phys. **85**, 3874 (1986).
[8] C.-L. Liao, R. Xu, and C. Y. Ng, J. Chem. Phys. **85**, 7136 (1986).
[9] J.-D. Shao, Y.-G. Li, G. D. Flesch, and C. Y. Ng, J. Chem. Phys. **86**, 170 (1987).
[10] K. Birkinshaw, A. Shukla, S. Howard, and J. H. Futrell, Chem. Phys. **113**, 149 (1987).
[11] R. H. Schultz and P. B. Armentrout, Chem. Phys. Lett. **179**, 429 (1991).
[12] D. M. Sonnenfroh and S. R. Leone, J. Chem. Phys. **90**, 1677 (1989).
[13] C. Rebrion, B. R. Rowe, and J. B. Marquette, J. Chem. Phys. **91**, 6142 (1989).
[14] M. Hawley and M. A. Smith, J. Phys. Chem. **96**, 6693 (1992).
[15] H.-S. Kim and M. T. Bowers, J. Chem. Phys. **93**, 1158 (1990).
[16] A. A. Viggiano, J. M. Van Doren, R. A. Morris, and J. F. Paulson, J. Chem. Phys. **93**, 4761 (1990).
[17] T. Kato, K. Tanaka, and I. Koyano, J. Chem. Phys. **77**, 337 (1982).
[18] M. Hamdan, K. Birkinshaw, and N. D. Twiddy, Int. J. Mass Spectrom. Ion Processes **57**, 225 (1984).
[19] P. M. Guyon, T. R. Gowers, and T. Baer, Z. Phys. D: At., Mol. Clusters **4**, 89 (1986).
[20] T. R. Govers, P. M. Guyon, T. Baer, K. Cole, H. Fröhlich, and M. Lavollée, Chem. Phys. **87**, 373 (1984).
[21] M. R. Spalburg, J. Los, and E. A. Gislason, Chem. Phys. **94**, 327 (1985).
[22] P. Archirel and B. Levy, Chem. Phys. **106**, 51 (1986).
[23] G. Parlant and E. A. Gislason, Chem. Phys. **101**, 227 (1986).
[24] G. Parlant and E. A. Gislason, J. Chem. Phys. **86**, 6183 (1987).
[25] E. E. Nikitin, M. Ya. Ovchinnikova, and D. V. Shalashilin, Chem. Phys. **111**, 313 (1987).
[26] G. Parlant and E. A. Gislason, J. Chem. Phys. **88**, 1633 (1988).
[27] D. C. Clary and D. M. Sonnenfroh, J. Chem. Phys. **90**, 1686 (1989).
[28] E. A. Gislason, G. Parlant, and M. Sizun, Adv. Chem. Phys. **82**, 321 (1992).
[29] V. Aquilanti, S. Cavalli, F. Pirani, A. Volpi, and D. Cappelletti, J. Phys. Chem. **105**, 2401 (2001).
[30] D. Cambi, D. Cappelletti, F. Pirani, and G. Liuti, J. Chem. Phys. **95**, 1852 (1991).
[31] D. Cappelletti, F. Pirani, and G. Liuti, Chem. Phys. Lett. **183**, 297 (1991).
[32] V. Aquilanti, D. Cappelletti, and F. Pirani, Chem. Phys. **209**, 299 (1996).
[33] V. Aquilanti, D. Cappelletti, and F. Pirani, Chem. Phys. Lett. **271**, 216 (1997); J. Chem. Phys. **106**, 5043 (1997); F. Pirani, A. Giulivi, D. Cappelletti, and V. Aquilanti, Mol. Phys. **98**, 1749 (2000).
[34] F. Pirani, D. Cappelletti, and G. Liuti (submitted).
[35] M.-L. Dubernet and J. M. Hutson, J. Chem. Phys. **101**, 1165 (1994).
[36] A. R. Edmonds, *Angular Momentum in Quantum Mechanics* (Princeton University Press, Princeton, 1980).
[37] V. Aquilanti and G. Grossi, J. Chem. Phys. **73**, 1165 (1980).
[38] V. Aquilanti, G. Liuti, F. Pirani, and F. Vecchiocattivi, J. Chem. Soc., Faraday Trans. 2 **85**, 955 (1989).
[39] F. Rebentrost and W. A. Lester, J. Chem. Phys. **64**, 3879 (1976).
[40] A. Carrington, C. A. Leach, A. J. Marr, A. M. Shaw, M. R. Viant, J. M. Hutson, and M. M. Law, J. Chem. Phys. **102**, 2379 (1995).
[41] J. L. Magee, J. Chem. Phys. **8**, 687 (1940).
[42] D. Rapp and W. E. Francis, J. Chem. Phys. **37**, 2631 (1962); B. M. Smirnov, Sov. Phys. Dokl. **10**, 218 (1965); R. E. Olson, F. T. Smith, and E. Bauer, Appl. Opt. **10**, 1848 (1970).
[43] R. Grice and D. R. Herschbach, Mol. Phys. **27**, 159 (1974).
[44] E. E. Nikitin, A. I. Reznikov, and S. Ya. Umanskii, Mol. Phys. **65**, 1301 (1988).
[45] J. H. Landenberg, I. B. Bucur, and P. Archirel, Chem. Phys. **221**, 225 (1997).
[46] H. H. Teng and D. C. Conway, J. Chem. Phys. **59**, 2316 (1973).
[47] E. Bauer, E. R. Fisher, and F. R. Gilmore, J. Chem. Phys. **51**, 4173 (1969).
[48] P. Tosi, O. Dmitrijev, Y. Soldo, D. Bassi, D. Cappelletti, F. Pirani, and V. Aquilanti, J. Chem. Phys. **99**, 985 (1993).
[49] L. D. Landau, Phys. Z. Sowjetunion **2**, 46 (1932).
[50] C. Zener, Proc. R. Soc. London, Ser. A **137**, 696 (1932).
[51] E. C. G. Stückelberg, Helv. Phys. Acta **5**, 369 (1932).
[52] Values of $R_x(\theta)$, $\Delta_x(\theta)$, and $E_x(\theta)$, features of $H(R,\theta)$ and detailed $P_{j\nu'}(E,\theta)$ formulas used in this analysis are provided by the authors on request.
[53] E. A. Gislason and Sachs, J. Chem. Phys. **62**, 2678 (1975).
[54] V. Aquilanti, R. Candori, F. Pirani, and Ch. Ottinger, Chem. Phys. **187**, 183 (1994).
[55] M. Halmann and I. Laulicht, J. Chem. Phys. **43**, 438 (1965).
[56] S. V. Bobashev and V. A. Kharchenko, *Electronic and Atomic Collisions*, book of abstracts, XVII ICPEAC, edited by I. E. McCarthy, W. R. McGillivray, and M. C. Sandage (Brisbane, 1991), p. 664; for previous applications to electronic-to-vibrational energy transfer, see Ref. 54, and to harpooning reactions, see M. De Castro, R. Candori, F. Pirani, V. Aquilanti, M. Garay, and A. G. Ureña, J. Phys. Chem. A **102**, 9537 (1998).
[57] M. De Castro, R. Candori, F. Pirani, V. Aquilanti, M. Garay, and A. G. Ureña, J. Chem. Phys. **112**, 770 (2000).
[58] F. F. McCormack, S. T. Pratt, J. L. Dehmer, and P. M. Dehmer, Phys. Rev. A **44**, 3007 (1991); K. P. Huber, Ch. Jungen, K. Yoshimo, K. Ito, and G. Stark, J. Chem. Phys. **100**, 7957 (1994).
[59] J. O. Hirschfelder, C. F. Curtis, and R. B. Bird, *Molecular Theory of Gases and Liquids* (Wiley, New York, 1967).
[60] V. Aquilanti, D. Ascenzi, M. Bartolomei, D. Cappelletti, S. Cavalli, M. De Castro Vitores, and F. Pirani, J. Am. Chem. Soc. **121**, 10794 (1999).
[61] D. Stogryn and A. Stogryn, Mol. Phys. **11**, 371 (1966).